X-ray emission cross sections following Ar^{18+} charge-exchange collisions on neutral argon: The role of the multiple electron capture

S. Otranto[1] and R. E. Olson[2]
[1]*CONICET and Dto. de Física, Universidad Nacional del Sur, 8000 Bahía Blanca, Argentina.*
[2]*Physics Department, Missouri University of Science and Technology, Rolla, Missouri 65401, USA*
(Received 9 December 2010; published 15 March 2011)

X-ray emission originating in charge-exchange collisions between Ar^{18+} and neutral argon is studied at impact energies of 5–4000 eV/amu by means of the classical trajectory Monte Carlo method (CTMC). Line emission and charge-exchange cross sections obtained from different CTMC versions based on the one-active electron approximation are contrasted among themselves and against the results obtained by means of a three-active electron code that lets us infer the role of multiple electron capture. The present results are compared to the recent experimental data available from the EBIT groups operating at Livermore, NIST, and Berlin. We were not able to reconcile the major difference in x-ray emission cross sections obtained from *in situ* measurements made in EBIT, versus those made in an exterior, field-free collision chamber using ions extracted from the EBIT. Our calculations support the extracted beam results.

DOI: 10.1103/PhysRevA.83.032710 PACS number(s): 34.70.+e, 32.30.Rj, 32.70.Fw, 95.30.Ky

I. INTRODUCTION

X-ray emission originating from charge-exchange collisions between highly charged ions and different atomic and molecular species has been found to be responsible for the cometary x-ray emission discovered by the German satellite ROSAT in 1996 (see [1] for a review). Since then, several laboratories worldwide as well as different theoretical groups have focused on this problem and have tried to reproduce these and other more recent astrophysical observations [2–7]. Besides the interest in increasing our understanding of such systems, there is also a practical application for the studies. There is a proposal to launch a solar wind observatory (SWO) satellite that could provide an instantaneous picture of future solar wind intensity and composition. With such an SWO orbiting Earth, cometary x-ray observations married to theoretical and experimental cross sections could predict disruptive solar wind ion activity in advance since the x-ray emissions precede by many hours the solar wind ions which travel at about 500 km/s. Such warnings could help prevent several reported solar-wind-induced problems, such as those in communication and navigational systems. Furthermore, the ion exposure risk to astronauts' health in spacewalks could be alleviated [8].

Theoretical work in the area has been mainly performed based on different versions of the classical trajectory Monte Carlo method (CTMC) [6,7,9–11]. The range of impact energies, the large projectile charges involved, and the multielectronic nature of the targets of interest make the implementation of quantum mechanical models based on expansions on atomic and molecular orbitals prohibitive. However, out of necessity, atomic hydrogen targets for projectiles with $q < 10$ have been occasionally employed to model the more complicated astrophysical data [12].

Concerning the laboratory experiments performed on the earth one can clearly distinguish between two different techniques. The more traditional approach is the one employed by the JPL group that uses an accelerator together with SiLi and Ge detectors to determine x-ray emissions from charge-exchange collisions [3]. Complementary data are obtained by the EBIT groups, like those available at LLNL, NIST, and Berlin, where the ion trap provides a unique access to these collision systems. One of the most noticeable advantages with EBIT measurements is that they are able to observe contributions to the spectra arising from long-lived forbidden transitions that cannot be seen with linear extraction lines. To exemplify, the $2\,^3S$ state has a lifetime of $\sim 10^{-3}$ s for O^{6+}, 3.9×10^{-3} s for C^{5+}, and 0.02 s for N^{4+} and decays into the $1\,^1S$ state via a relativistic magnetic dipole transition. At the typical solar wind velocities of 450–750 km/s it then takes the O^{6+} ion $2\,^3S$ state about 0.45–0.75 km to decay to the $1\,^1S$ state, a distance much larger than the dimensions of any collision chamber.

On the other hand, EBIT results have two main limitations: (a) Most of the reported data have been collected in the magnetic trapping mode with collision energies restricted to the range of 10–25 eV/amu [i.e., far below the solar wind energies (1–3 keV/amu)]; (b) the reported uncertainty for the collision energy in this operating mode is about 50% [13,14], and the resulting collision energy distribution is unmeasured.

Another option explored by the NIST and Berlin groups is to use the EBIT as an ion source, then extract, filter, and direct the produced ions onto a target gas in a separate, exterior collision chamber [14,15]. Although this removes the chance of measuring forbidden transitions, the technique allows the extension of impact energy to the range corresponding to that of solar wind ions.

By direct comparison of the obtained spectra and the hardness ratio values at different collision energies, the Berlin group has recently reported significant discrepancies (factor of two) in the emission cross sections measured *in situ* in the EBIT with those obtained once the beam is extracted. The main differences are seen at the lower impact energies (5–18 eV/amu) and imply a significant difference in the (n,l) population of the final states of the projectile. To our knowledge, this major discrepancy remains unclarified.

In our work we explore the Ar^{18+} + Ar collision system because of the availability of both EBIT and extracted beam measurements. This is a difficult system because it is well

known since the 1970s that the eight electrons in the M shell of the Ar atom provide abundant opportunity for multiple electron transitions in energetic collisions [16–18]. Furthermore, since electron capture is primarily an exoergic process, even at very low collision energies multiple capture is exceedingly important since it is driven by the potential energy available in the multiply charged ion, not the kinetic energy that the ion possesses.

For this investigation we will be using the CTMC method. In particular, results obtained with several three-body codes which consider one active electron are contrasted among themselves and against a five-body code which incorporates three active electrons as described in the next section. Special emphasis is made on the role of multiple charge exchange; autoionizing double and triple capture as well as radiative double-electron capture are considered. Line emission cross sections are shown and contrasted to the Berlin and NIST data, and the main conclusions and outlook are summarized.

II. THEORETICAL METHOD

For decades it has been suggested that the success of the CTMC model describing processes involving atomic hydrogen as a target can be attached to the fact that the classical momentum distribution for atomic hydrogen is exactly equivalent to the quantum mechanical one [19]. Charge-exchange collisions, in particular, are primarily determined by velocity matching between the incoming projectile and the target electron, reinforcing the idea that a proper description of the electronic momentum distribution is critical in order to obtain reasonable results. The hydrogenic approximation has been used for decades as a fast and easy alternative to explore more complex systems (molecules, multielectronic atoms) within the CTMC model, and even non-Coulombic potentials have been widely used to provide a more precise description of the electron-target interactions [20,21]. Multielectronic targets in general lead to inaccurate momentum distributions when events are initially sorted over the radial distributions and the corresponding electronic momentum values are obtained by means of the energy equation.

In a recent article [9], we considered the H_2O target and used the expansions in terms of Slater functions provided by Moccia for the different orbitals [22] in order to get their spherically averaged quantum mechanical momentum distributions. Furthermore, we have shown that by sorting events over these momentum distributions even the radial distributions could be improved, avoiding the deficiencies typical of the microcanonical distributions.

In this work we are using three versions of the three-body CTMC code:

(1) Hydrogenic model. In this model, the bound electron evolves around the target nucleus subject to a Coulomb potential $-1/r$. In this sense this model resembles the hydrogen atom and different targets are considered only through their respective ionization potentials.

(2) Central potential model. In this model the electron evolves under the target field corresponding to a model potential derived from Hartree-Fock calculations for the $3p$ state of neutral Ar [Ar($3p$)] [23]. Although still a three-body model, this treatment should be much more accurate since the active electron is treated on a much more realistic basis and sees an r-dependent nuclear charge which goes from $+18$ in the limit $r \to 0$ up to $+1$ in the limit $r \to \infty$.

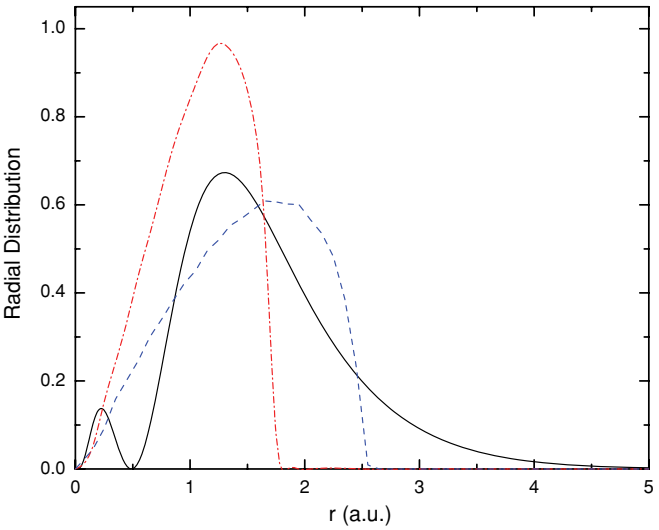

FIG. 1. (Color online) Radial distributions for Ar($3p$). Solid line, quantum mechanical result; dot-dashed line, model 1; dashed line, model 2.

(3) The CTMC model introduced in Ref. [9] in which events are sorted over the quantum mechanical momentum distribution corresponding to the Ar($3p$) and the electron evolves subject to a hydrogenic target potential with an effective charge which is set in order to provide the best possible agreement with the quantum mechanical radial distribution. The corresponding radial and momentum distributions obtained with the first two models are shown in Fig. 1 and compared to the quantum mechanical result. It can be seen that model 3 leads to a radial distribution that is in much better agreement with the quantum mechanical one compared to models 1 and 2.

Since multiple capture events are expected to play a role in this collision system we are also using a five-body CTMC code in which the electrons are sorted with sequential binding energies over the quantum mechanical momentum distributions corresponding to the Ar($3p$), Ar^+($3p$), and Ar^{2+}($3p$) states for which we use the expansions provided by Clementi and Roetti [24]. Hydrogenic potentials with individual effective charges set in order to provide the best agreement with the quantum mechanical radial distributions are employed for the corresponding electron-target interactions. Figure 2 shows the obtained radial distributions for the three electrons compared to their quantum mechanical counterparts. This model will be termed hereafter as model 4.

As usual in the CTMC model, charge-exchange processes are classified according to the classical number $n_c$that is obtained from the binding energy E_p of the electron relative to the projectile by

$$E_p = -Z_p^2/\left(2n_c^2\right). \tag{1}$$

Then, n_c is related to the quantum number n of the final state by the condition,

$$[(n-1)(n-1/2)n]^{1/3} \leqslant n_c \leqslant [n(n+1)(n+1/2)]^{1/3}. \tag{2}$$

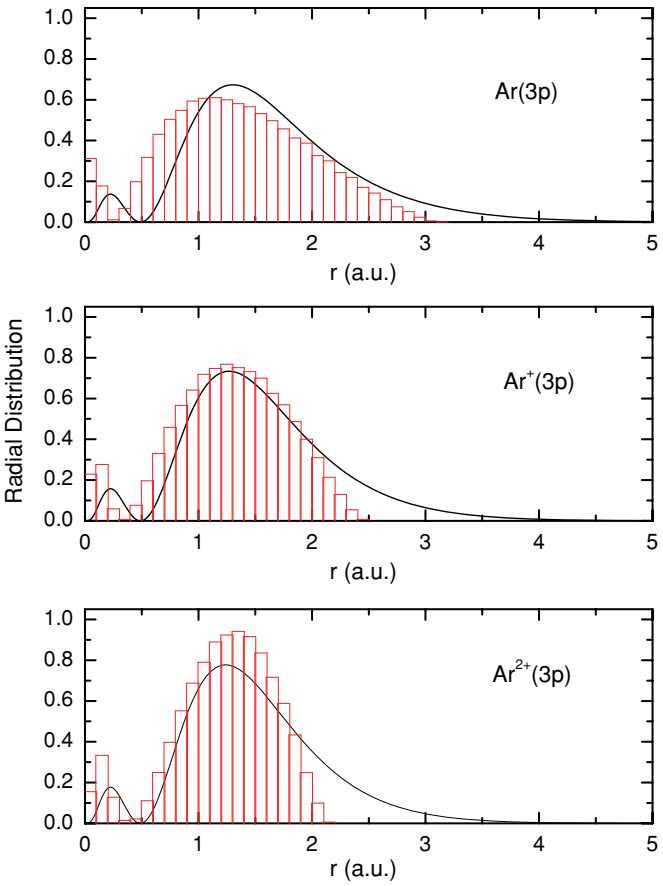

FIG. 2. (Color online) Radial distributions for Ar(3p), $Ar^{+}(3p)$, and $Ar^{2+}(3p)$. Solid line, quantum mechanical result; bars, present CTMC model in which events are sorted over the quantum mechanical momentum distribution (model 3).

Multiple capture is treated in the present five-body model as follows: double-capture events to levels n_1 and n_2 for which $|n_1 - n_2| \leqslant 1$ are assumed to lead to autoionizing double capture [15], which is also sometimes termed transfer ionization.

$$\begin{aligned} Ar^{18+} + Ar &\rightarrow Ar^{16+*}(n_1l_1,n_2l_2) + Ar^{2+} \\ &\rightarrow Ar^{17+*}(n,l) + e + Ar^{2+} \\ &\rightarrow Ar^{17+}(1s) + h\nu_1 + e + Ar^{2+}. \end{aligned} \quad (3)$$

The electron with the greater n_c value is considered to autoionize with zero energy; conserving energy the inner one falls to a deeper n value and its l value is modified by preserving the orbital eccentricity. Even if the electrons' roles are reversed, the final orbital energy is unchanged. Thus, in autoionizing double capture, the resultant argon ion is singly charged, just as in true single-electron capture. However, the line emission after the Auger process arises from a lower n value than in true single capture.

Events for which $|n_1 - n_2| > 1$ are treated as radiative decay and the decay routes of both electrons are explicitly considered. For radiative double capture,

$$\begin{aligned} Ar^{18+} + Ar &\rightarrow Ar^{16+*}(n_1l_1,n_2l_2) + Ar^{2+} \\ &\rightarrow Ar^{16+}(1s^2) + h\nu_1 + h\nu_2 + Ar^{2+}, \end{aligned} \quad (4)$$

two sequences of line emission are obtained, one from the lower n value and one from the larger n value. The electronic energy structure corresponds to that of Ar^{16+}. The most notable feature is that instead of obtaining a Ly-α line at 3306 eV like in single charge exchange or autoionizing double capture, the successive decays lead to a shoulder that is located on the low-energy side of the dominant Ar^{17+} ($2p \rightarrow 1s$) transition peak.

For three-electron capture, we have observed that most of the events correspond to two electrons bound with nearly equal n values while the third one is bound to a greater n' value. We have assumed these events decay according to the following scheme: the two electrons with the greatest n_c values are emitted to the continuum (autoionize) with zero energy while the third inner one falls to a deeper n level preserving orbital eccentricity and conserving energy:

$$\begin{aligned} Ar^{18+} + Ar &\rightarrow Ar^{15+*}(n_1l_1,n_2l_2,n_3l_3) + Ar^{3+} \\ &\rightarrow Ar^{17+*}(n,l) + e_1 + e_2 + Ar^{3+} \\ &\rightarrow Ar^{17+}(1s) + h\nu + e_1 + e_2 + Ar^{3+}. \end{aligned} \quad (5)$$

In all cases the emission cross sections are obtained following a similar procedure to that given in Ref. [6].

III. RESULTS

We will first describe the charge-exchange transition probabilities as a function of impact parameter at the collision energy of 1 keV/amu. In Fig. 3, we show the results obtained with the three-body codes described above. It can be seen that model 1 describes the charge-exchange processes over a more limited range of impact parameters than the CTMC models based either on a central potential for the active electron-target nucleus interaction (model 2) or on the correct quantum mechanical momentum distribution (model 3). These two models provide distributions that are close to each other

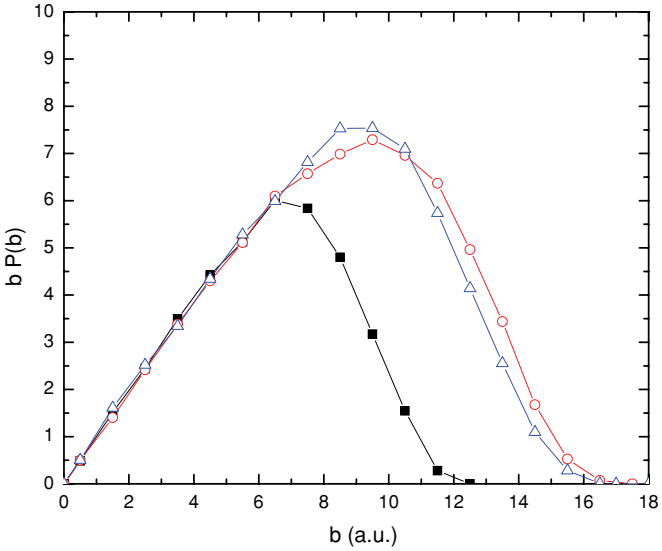

FIG. 3. (Color online) Charge-exchange distributions as a function of impact pact parameter at 1 keV/amu for Ar(3p) using the three-body CTMC models. Squares, model 1; open circles, model 2; open triangles, model 3.

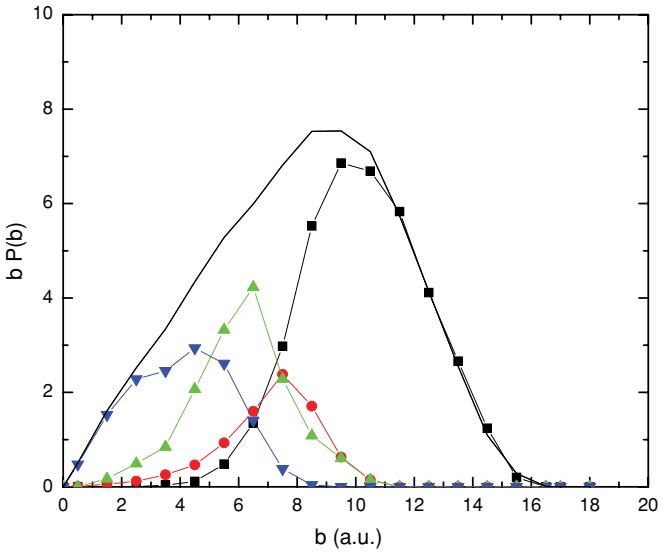

FIG. 4. (Color online) Charge-exchange distributions as a function of impact parameter at 1 keV/amu for Ar($3p$) using model 4. Results are contrasted to the three-body code sorted over the correct momentum distribution (model 3). Solid line, model 3; squares, single-electron capture; circles, double capture with autoionization; up-triangles, double capture followed by radiative decay; down-triangles, triple capture with autoionization.

and extend the capture probabilities to impact parameters from 12 a.u. to about 17 a.u. due to the increased range of target radial electron density. Due to the larger range of interaction, the more accurate radial distributions display an increased total cross section of 1.2×10^{-14} cm^2 versus that of the simple hydrogenic approximation which yields 7.0×10^{-15} cm^2. We will also see later that the longer range of interaction leads to preferentially populating higher levels of the Ar^+ ion, $n =$ 9–10, than in the hydrogenic case, $n = 8$.

In Fig. 4 we compare the impact parameter transition probabilities for the single and multiple capture channels. Model 3 is compared to model 4. As we said before, these models share the description of the outer Ar($3p$) electron but they differ in the number of active electrons under consideration. The large impact parameters clearly contribute to the single charge-exchange channel, while the smaller impact parameters mainly lead to initial double and triple capture. As previously indicated, double capture is separated in terms of autoionizing double capture, final state Ar^{17+}, and double radiative decay, final state Ar^{16+}. It can be seen that at the largest impact parameters (12–17 a.u.), models 3 and 4 are in agreement. For the lower impact parameter hard collisions, initial double and triple capture channels dominate. In this region, model 3 leads to single charge exchange which hides the multiple electron collision dynamics. For impact parameters smaller than 4 a.u., model 3 results for single charge exchange are replaced by autoionizing triple capture, this being the primary channel feeding those impact parameters in model 4.

In Fig. 5, n-selective cross sections are presented at the collision energy of 1 keV/amu. In Fig. 5(a), results obtained with models 1–3 are displayed. The hydrogenic CTMC model clearly peaks in accordance with the scaling $\sqrt{13.6/V_{\rm ion}}Z_p^{3/4}$

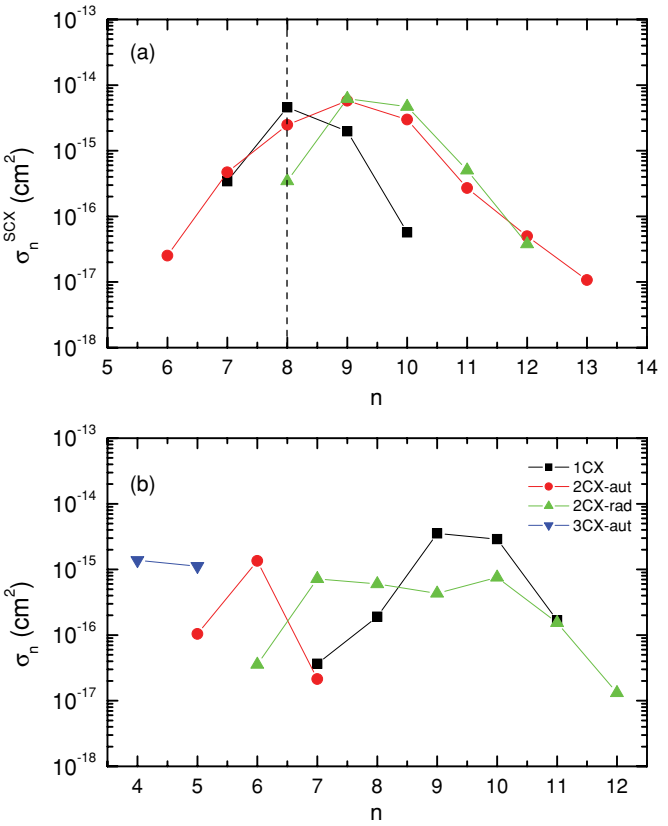

FIG. 5. (Color online) n distributions at 1 keV/amu for Ar^{18+} + Ar. (a) Results obtained with the present three-body codes are as follows: squares, model 1; circles, model 2; triangles, model 3. The dashed line indicates the $n_{\rm max}$ position predicted by the scaling law $\sqrt{13.6/V_{\rm ion}}Z_p^{3/4}$; (b) results obtained with model 4.

which for a projectile charge of 18+ leads to $n_{\rm max} = 8$ [25]. Models 2 and 3, both exhibit a peak at $n_{\rm max} =$ 9–10 and result in a wider distribution.

Results obtained with model 4 are shown in Fig. 5(b). The single charge-exchange distributions peaks at $n =$ 9–10 in accord with the more elaborate three-body codes. Double capture leading to radiative decay exhibits two peaks, one associated with the outer electron ($n = 10$) and one associated with the capture of an inner electron ($n = 7$). On the other hand, autoionizing double and triple capture peak at inner n values as expected ($n = 6$ and $n =$ 4–5, respectively).

Although the above comparisons between various theoretical models can be very instructive, the merit of any theoretical description can only be assessed by benchmarking it against experimental measurements. A nice set of line emission spectra are now available from the Berlin EBIT group. These data are further supplemented by NIST EBIT measurements.

In both locations, Ar^{18+} ions produced in the EBIT trap were extracted and line emission measurements were made in an exterior collision chamber. The Berlin group also measured the line spectra *in situ* in the EBIT and compared them to the extracted beam results. The hardness ratio, that is, the fraction of the $np \rightarrow 1s$ for $n > 2$ line emissions divided by the intensity for the Lyman-α transition, was found to differ

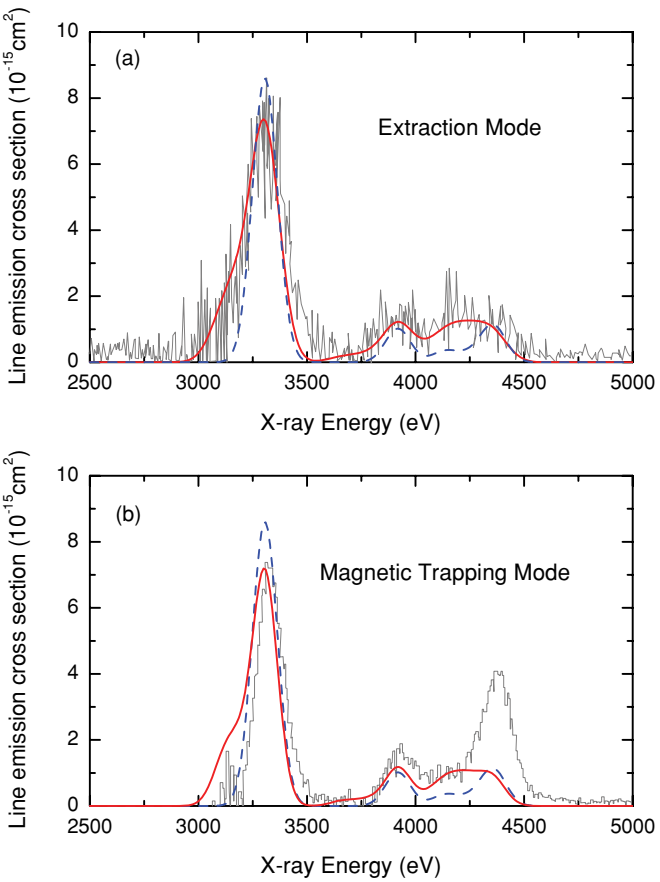

FIG. 6. (Color online) Line emission cross sections for 18 eV/amu Ar^{18+} + Ar collisions. Thick solid line, model 4 results; dashed line, model 3 results; thin solid line, experimental data of Allen *et al*. (Ref. [14]) operating the EBIT in (a) extraction mode and (b) magnetic trapping mode.

by a factor of two between the two sets of measurements. No explanation is given for the disagreement. It should also be noted that the Berlin *in situ* hardness ratio measurements are in very good agreement with similar results obtained at the Livermore EBIT [13].

In Fig. 6 we compare our theoretical results to the Berlin data measured at 18 eV/amu. In this case, both extracted beam and *in situ* line emission spectra are available. In order to compare to the data, we have convoluted our theoretical line emission cross sections with Gaussian functions having a full width at half maximum (FWHM) of 168 eV (to reproduce the reported resolution for the spectrometer operating in the extraction mode) and 136 eV (for the resolution of the spectrometer operating in the magnetic trapping mode). First, comparing the results obtained with model 3 against those obtained with model 4, that include multiple capture, we see major difference in the shapes of the spectra. Model 3 does not display the increased intensity in the line emission due to the 4,5 $\rightarrow$ 1 transitions that are fed by multiple capture. Moreover, the multiple capture results display a "shoulder" on the low-energy side of the Lyman-α peak. The latter is a consequence of double capture followed by radiative decay of the two-electron ion. Thus, this "shoulder" on the Lyman-α peak appears to be a direct signature of multiple capture. Figure 6(a) shows the extracted beam data, while Fig. 6(b) displays the *in situ* measurements. Our calculations clearly favor the extracted beam results where good agreement is realized with the data. The *in situ* measurements [Fig. 6(b)] display very pronounced $9p$,$10p \rightarrow 1s$ line emission that we cannot reproduce, but is in agreement with similar spectra measured at LLNL [13].

An uncertainty with the *in situ* EBIT measurements is that the nominal energy can only be estimated to about 50%. Moreover, the collision energy distribution is unknown and will most likely differ considerably from the usual Boltzmann distribution. However, when we varied the collision energy by an order of magnitude, only very minor changes were found in the line emission; thus, we cannot ascribe the discrepancy between the observations to the energy dependence of the cross sections. Since the CTMC model also yields n,l,m distributions [26], we investigated alignment effects since the beam measurements have a defined collision direction while the EBIT measurements do not. Again, we were unsuccessful in finding significant changes in the cross sections. An electric field was also included in the three-body results [27], and again no significant changes in the cross sections were found for reasonable field strengths. Hence, it appears that the only experimental variable left unstudied is the magnetic fields inherent in the *in situ* EBIT trap measurements.

Unrelated to the collision dynamics, there is an additional uncertainty imposed on the *in situ* EBIT measurements that is related to the analysis of the data. In an EBIT, spectra for all ion charge states are collected at the same time. If one is investigating line emission from collisions involving bare ions, such as the case here, the ion spectra for lower charge states are manually subtracted from the data. By so doing, an assumption is made that only single-electron final state capture occurs. However, we find that double capture followed by radiative decay as in reaction (4) does lead to observable cross sections. The *in situ* EBIT analysis removes these events thereby artificially lowering the Lyman-α peak signal. Since multiple capture followed by radiative decay processes become increasingly important for high charge states, the comparison between theory and experiment become tenuous. It is quite possible that the analysis procedure is responsible for the apparent disagreement between theory and experiment in the hardness ratio as the Z of the ion increases [13].

In Fig. 7 we compare our calculations to the Berlin extracted beam data at 5, 218, and 2140 eV/amu. Again excellent agreement is observed and the shoulder on the Lyman-α peak, the signature of radiative multiple capture, is clearly reproduced in our multielectron calculations. When we compare to the NIST data at 4 keV/amu (130 eV resolution), the high $n \rightarrow 1$ transitions are well reproduced, but we underestimate the intermediate peak due to the $3p \rightarrow 1s$ transition. A hint of this trend is also apparent in the 2140 eV/amu Berlin data. This is probably due to our neglect of higher degrees of initial multiple capture. It is well known since the pioneering measurements of Mueller and Salzborn that very high levels of multiple electron removal exist for keV/amu collisions of highly charged ions with the heavier rare gases [28].

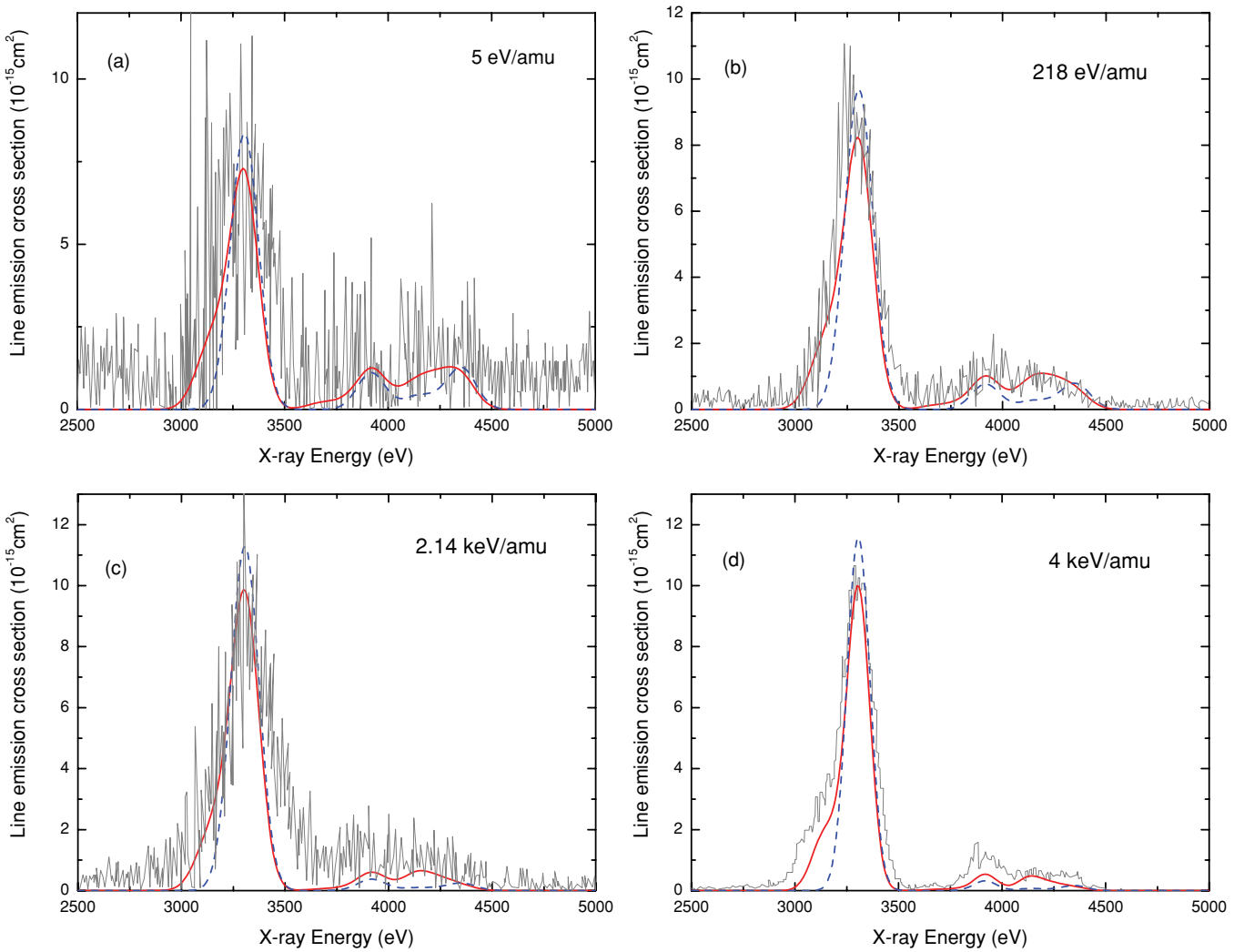

FIG. 7. (Color online) Line emission cross sections for 5 eV/amu, 218 eV/amu, 2.14 keV/amu, and 4 keV/amu Ar^{18+} + Ar collisions. Thick solid line, model 4 results; dashed line, model 3 results; thin solid line, experimental data from Allen *et al.* (2008) [14] [Figs. 7(a)–7(c)], and Tawara *et al.* [15] (2006) [Fig. 7(d)].

IV. CONCLUSIONS

In this work we have studied the Ar^{18+} + Ar collision system at impact energies in the range of 5eV/amu to 4 keV/amu by means of CTMC models. Previous three-body models were discussed and compared to a five-body model in which autoionizing double capture, radiative decay double capture, and autoionizing triple capture have been explicitly considered. These multiple electron capture channels redistribute their final *n,l* levels before radiative decay via x-ray emission. Although their summed total cross sections vary little from the three-body results, major changes are observed in the line emission cross sections. These multiple electron capture channels redistribute the final *n,l* levels before radiative decay via x-ray emission. As a result, comparison to line emission data indicates a more realistic description of the collision system.

However, in our studies we were not able to reconcile in the collision dynamics for the major difference in x-ray emission cross sections obtained from *in situ* measurements made in EBIT [13,14], versus those made in an exterior, field-free collision chamber using ions extracted from the EBIT [14,15]. Electric fields were investigated along with possible alignment effects that turned out to be negligible. The energy dependence of the line emission cross sections was also removed from consideration. At this point the only experimental variable that remains unstudied are the magnetic fields inside an EBIT ion trap. However, we do point out the questionable analysis of *in situ* measurements that removes multiple radiative electron capture from inclusion in the data [i.e., reaction (4) above].

Our five-body code results clearly support the extracted beam results and lead to line emission cross sections in good agreement to those measured at the Berlin EBIT at impact energies of 5, 18, 218, and 2140 eV/amu and those obtained at NIST at 4 keV/amu. The clear signature of multiple radiative capture is displayed by the presence of a "shoulder" on the Lyman-α peak. In contrast, the three-body descriptions clearly underestimate the higher Lyman lines and ignore multiple capture features. Further experimental studies would be welcome to help clarify this elusive topic.

ACKNOWLEDGMENTS

Work at Universidad Nacional del Sur is supported by Grants No. PGI 24/F049, No. PICT-2007-00887 of the ANPCyT, and No. PIP 112-200801-02760 of CONICET (Argentina).

[1] T. E. Cravens, Science **296**, 1042 (2002).
[2] J. B. Greenwood, I. D. Williams, S. J. Smith, and A. Chutjian, Astrophys. J. Lett. **533**, L175 (2000).
[3] J. B. Greenwood, I. D. Williams, S. J. Smith, and A. Chutjian, Phys. Rev. A **63**, 062707 (2001).
[4] P. Beiersdorfer *et al.*, Science **300**, 1558 (2003).
[5] V. Kharchenko, Matt Rigazio, A. Dalgarno, and V. A. Krasnopolsky, Astrophys. J. **585**, L73 (2003).
[6] S. Otranto, R. E. Olson, and P. Beiersdorfer, Phys. Rev. A **73**, 022723 (2006).
[7] S. Otranto, R. E. Olson, and P. Beiersdorfer, J. Phys. B **40**, 1755 (2007).
[8] *1997 Space Weather: A Research Perspective* (National Academy of Sciences Report, Washington, DC, 1997).
[9] S. Otranto and R. E. Olson, Phys. Rev. A **77**, 022709 (2008).
[10] J. Simcic, D. R. Schultz, R. J. Mawhorter, I. Cadez, J. B. Greenwood, A. Chutjian, C. M. Lisse, and S. J. Smith, Phys. Rev. A **81**, 062715 (2010).
[11] R. Ali, P. A. Neill, P. Beiersdorfer, C. L. Harris, D. R. Schultz, and P. C. Stancil, Astr. J. **716**, L95 (2010).
[12] D. Bodewits, R. Hoekstra, B. Seredyuk, R. W. McCullough, G. H. Jones, and A. G. G. M. Tielens, Astrophys. J. **642**, 593 (2006).
[13] P. Beiersdorfer, R. E. Olson, G. V. Brown, H. Chen, C. L. Harris, P. A. Neill, L. Schweikhard, S. B. Utter, and K. Widmann, Phys. Rev. Lett. **85**, 5090 (2000).
[14] F. I. Allen, C. Biedermann, R. Radtke, G. Fussmann, and S. Fritzsche, Phys. Rev. A **78**, 032705 (2008).
[15] H. Tawara, E. Takács, T. Suta, K. Makónyi, L. P. Ratliff, and J. D. Gillaspy, Phys. Rev. A **73**, 012704 (2006).
[16] A. S. Schlachter, K. H. Berkner, W. G. Graham, R. V. Pyle, P. J. Schneider, K. R. Stalder, J. W. Stearns, J. A. Tanis, and R. E. Olson, Phys. Rev. A **23**, 2331 (1981).
[17] A. Müller, B. Schuch, W. Groh, E. Salzborn, H. F. Beyer, P. H. Mokler, and R. E. Olson, Phys. Rev. A **33**, 3010 (1986).
[18] R. E. Olson, J. Ullrich, and H. Schmidt-Bocking, Phys. Rev. A **39**, 5572 (1989).
[19] R. Abrines and I. C. Percival, Proc. Phys. Soc. London **88**, 873 (1966).
[20] C. O. Reinhold and C. A. Falcon, Phys. Rev. A **33**, 3859 (1986).
[21] R. E. Olson, *Springer Handbook of Atomic, Molecular and Optical Physics* (Springer, New York, 2006).
[22] R. Moccia, J. Chem. Phys. **40**, 2186 (1964).
[23] J. E. Miraglia, Phys. Rev. A **79**, 022708 (2009).
[24] E. Clementi and C. Roetti, At. Data Nucl. Data Tables **14**, 177 (1974).
[25] R. E. Olson, J. Phys. B: Atom. Molec. Opt. Phys. **12**, 1843 (1979).
[26] S. Schippers, P. Boduch, J. van Buchem, F. W. Bliek, R. Hoekstra, R. Morgenstern, and R. E. Olson, J. Phys. B: At. Mol. Opt. Phys. **28**, 3271 (1995).
[27] C. R. Feeler and R. E. Olson, J. Phys. B: At. Mol. Opt. Phys. **33**, 1997 (2000).
[28] A. Mueller and E. Salzborn, Phys. Lett. **62**, A391 (1977).